ADVANCED FUNCTIONAL MATERIALS
www.afm-journal.de

Gold Core-DNA-Silver Shell Nanoparticles with Intense Plasmonic Chiroptical Activities

Xiaoling Wu, Liguang Xu, Wei Ma, Liqiang Liu, Hua Kuang, Wenjing Yan, Libing Wang, and Chuanlai Xu*

The strong plasmonic chiroptical activities of gold core-DNA-silver shell nanoparticles (NPs) are reported for the first time, using cytosine-rich single-stranded DNA as the template for the guidance of silver shell growth. The anisotropy factor of the optically active NPs at 420 nm reaches 1.93×10^{-2}. Their chiroptical properties are likely induced by the DNA–plasmon interaction and markedly amplified by the strong electromagnetic coupling between the gold core and silver shell.

1. Introduction

Chiral metal nanoparticles (NPs) exhibit unique circular dichroism (CD) in the plasmonic parts of the spectrum, and have gained extensive scientific attention.[1] The majority of plasmonic optically active NPs have primarily been sub-nanometer clusters with the protecting ligands capping the metal centers during the growth process.[1a-c] A few studies have reported optically active NPs by adsorbing the chiral molecules on the surface of naked metal NPs.[2] However, their chiroptical properties, particularly in the plasmonic regions, are weak and vulnerable to environmental conditions, which restrict their applications.[3]

Nanomaterials based on DNA nanotechnology are currently one of the most dynamic research areas.[3a,4] Following the DNA template, a variety of metal nanowires and nanoclusters has been formed by the reduction of DNA-complexed metal ions.[5] Due to the high affinity between silver ions (Ag^+) and DNA, Ag nanoclusters and NPs grown on DNA scaffolds have particularly attracted the interest of researchers.[6] However, the majority of these studies have concentrated on the growth of Ag clusters on the DNA template[6b,d,7] and their fluorescence features.[5d,6a] Markovich and co-workers reported the synthesis of Ag NPs on the DNA framework, and observed very weak CD signals, while the origin of the chiroplasmonic signal was unclear.[6e,8] Our group fabricated shell-engineered chiroplasmonic assemblies, and demonstrated that the deposition of silver shell around the optically active NP heterodimers enhanced the plasmonic CD signal.[9] However, there are no reports, to date, on DNA-driven individual NPs with intense chiroplasmonic activity.

Herein, we successfully achieved gold core-DNA-silver shell NPs, namely, Au/(DNA-Ag) core–shell NPs, with Ag grown on the DNA template (DNA-Ag). The obtained NPs exhibited an intense and robust chiroptical response at the Ag plasmon band, and the plasmonic chirogenesis of NPs was revealed.

2. Results and Discussion

Optically active Au/(DNA-Ag) core–shell NPs were prepared under a DNA-template growth process, and cytosine-rich DNAs (DNA 1 in Table S1, Supporting Information) were intentionally chosen in this study.[6b] To prepare the Au/(DNA-Ag) core–shell NPs, as-prepared gold NPs core (Au NPs) were first modified with an excess concentration of C_{30} thiolated single-stranded (ss) DNA (Au NPs-DNA) to guarantee saturation of all possible Au NPs binding sites. Then silver ions (Ag^+) were strongly bound to the C_{30} ssDNA scaffolds by adding silver nitrate ($AgNO_3$) to the solution, leading to the formation of metal complexes (Au/DNA-Ag^+). An additional centrifugation process was then required to remove the excess Ag^+. Therefore, only those binding Ag^+ were ultimately transformed to a dense Ag shell on the surface of each Au NP by the chemical reducing agent, ascorbic acid (**Figure 1**), and the Au/(DNA-Ag) core–shell NPs were finally prepared.

By adjusting the amount of $AgNO_3$ solution, an Ag shell of varying thickness was formed on the surface of the Au NP, which was verified by transmission electron microscopy (TEM, **Figure 2**A) and energy-dispersive X-ray spectroscopy (EDX, Figure S1, Supporting Information). According to an extensive analysis of TEM images (Figure 2A and Figure S2, Supporting Information), the Ag shell thickness was calculated to increase gradually from 0.4 ± 0.1 to 8.0 ± 0.6 nm on the Au core (Figure S3A, Supporting Information), by the addition of 5, 10, 30, 40, and 50 µL of 0.75×10^{-3} M $AgNO_3$ solution, respectively. A maximum value (8.0 ± 0.6 nm) was observed when the volume of $AgNO_3$ added reached more than 40 µL, due to the maximum loading amount of DNA on the Au NP,[10] and the saturation binding ability of Ag^+ to ssDNA.[6b] In comparison, when the cytosine-rich ssDNAs were replaced with the thymine-rich ssDNAs, the Ag shell thickness of the obtained NPs was 5.11 ± 0.05 nm (Figure S4, Supporting Information).[6b,11] Correspondingly, the percentage of Ag element of Au/(DNA-Ag) core–shell NPs was identified to increase from 20% to

X. Wu, L. Xu, W. Ma, L. Liu, Prof. H. Kuang, W. Yan, Prof. L. Wang, Prof. C. Xu
State Key Lab of Food Science and Technology
School of Food Science and Technology
Jiangnan University
Wuxi, Jiangsu Province 214122, China
E-mail: kuangh@jiangnan.edu.cn

DOI: 10.1002/adfm.201403161

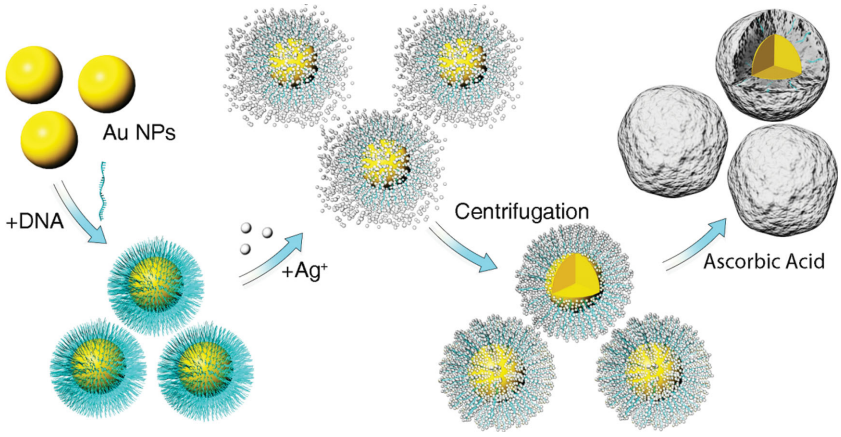

Figure 1. Schematic illustration for the synthesis of optically active gold core-DNA-silver shell NPs.

57.5% as shown by EDX measurements (Figure S1, Supporting Information). As shown from the dynamic light scattering measurements in Figure S3B, Supporting Information, these obtained NPs were stable and well-dispersed without aggregation. And based on the statistical analysis of bright-field TEM images (Figure S5, Supporting Information), the achieved Au/(DNA-Ag) core–shell NPs (40 μL of $AgNO_3$ solution) were formed in high yield of 99.21% ± 1.31%, with minimal amount of Au NPs remaining as freely suspended colloids.

The structures with varying shell thickness, showed marked changes in optical activity (Figure 2B). As the Ag shell became thicker, the 400 nm (the peak of the Ag plasmon resonance band) absorption peak appeared, and became more dominant.[12] Synchronously, with their varying absorption properties, a large increase in chiroptical activity was observed at 413 nm with slightly red shift (7 nm) (Figure 2B). When the thickness of the Ag shell was 8.0 ± 0.6 nm, the CD signal at 420 nm reached 105 ± 2.3 mdeg, with the chiral anisotropy factor, *g*, of the NPs equal to 1.93×10^{-2} (Figure 2C). This is quite impressive for individual NPs and the *g*-factor value is approximately 1 order of magnitude higher than that of plasmonic or nonplasmonic nanoclusters or NPs (Table S2, Supporting Information).[1a,2,13], It is well comparable with one of the highest, obtained to date, for NPs assembly systems.[4d,14]

In order to address the origin of the intense chiroplasmonic activity of the Au/(DNA-Ag) core–shell NPs, we initially tracked the chiroptical response of the components of the NPs, following the growth process (**Figure 3**A, B). As shown in Figure 3A, the starting cores of Au NPs were achiral, and displayed no chiroptical signature. The Au cores attached to DNA (Au NPs-DNA) showed weak chiroplasmonic absorption (0.46 ± 0.1 mdeg) appeared only in the range of 500–550 nm, due to the induction from electronic "imprinting" of the Au core by conjugating DNA.[15] And Au NPs-DNA bound with Ag^+ (Au/DNA-Ag^+) exhibited a similar chiral shape of Au NPs-DNA in the plamonic region of CD spectrum. All the tested cases, before final growth of the Ag shell, showed no plasmonic optical activity or weak CD bands at 500–550 nm.

To clarify the chiral mechanism of Au/(DNA-Ag) core–shell NPs, we performed three control experiments. First, Au–Ag core–shell NPs without DNA, which were named Au@Ag NPs, were synthesized by depositing the Ag shell onto the Au NP core (Figure S6, Supporting Information).[9,12a] As shown in Figure 3A, the naked Au@Ag NPs showed no chiral absorption at all. Second, Au@Ag NPs were functionalized with DNAs (DNA 1 in Table S1, Supporting Information), and the CD intensity around 400 nm was 0.9 ± 0.1 mdeg (Figure 3A). Third, we prepared Ag NPs grown on the DNA template without Au core, denoted as DNA-Ag NPs (DNA 1 in Table S1 and Figure S7, Supporting Information). They showed a weak CD signal of 2.5 ± 0.2 mdeg at 428 nm (Figure 3A), corresponding with the early study.[6e]

From the results in Figure 3C,D, it was clearly showed that the high-resolution TEM (HRTEM) images of Au@Ag NPs (Figure 3C) were dramatically different to those of Au/(DNA-Ag) core–shell NPs (Figure 3D). The Ag shells of Au@Ag NPs had seemingly been epitaxially deposited on the Au NP surface and presented uniform single-crystalline structures with the (111) bare surfaces.[16] Comparably, Au/(DNA-Ag) core–shell NPs displayed polycrystalline structures and dominated by the (111) facets with a corresponding lattice spacing of 0.23 nm[17] (Figure 3D), where the chiral DNAs were embedded in the Ag shells during the growth process, and strongly disturbed the epitaxial growth of the Ag shells.

For further understanding the chirogenesis of Au/(DNA-Ag) core–shell NPs, the hetero-trimers, denoted as Au-(DNA-Ag)-Au trimers were also constructed (**Figure 4** and Figure S8, Supporting Information).[6b] As shown in Figure 4A, the Au-(DNA-Ag)-Au trimers showed a CD band of 8.43 ± 0.7 mdeg at 529 nm located at the position of Au plasmon resonance band, which was originated from the prolate shape of NPs with a consistent dihedral angle[14,18] of Au NP homodimers, and enhanced by the electromagnetic coupling of Au NP homodimers and (DNA-Ag) NPs (Figure S9, Supporting Information). Following the growth of (DNA-Ag) NPs, a new band, positioned at the Ag plasmon band appeared. The CD signal at 408 nm was 5.1 ± 0.5 mdeg, which was approximately 20.6 times lower than that of Au/(DNA-Ag) core–shell NPs. The stronger CD intensity of Au/(DNA-Ag) core–shell NPs should be attributed to the high amount of DNA in the grown shells of Au/(DNA-Ag) core–shell NPs and the core–shell enhanced electric field produced strong chiroplasmonic activity (Figure S9, Supporting Information). The effect of high amount of DNA as chiral source is dominant for contributing the strong chiroptical activity for Au/(DNA-Ag) core–shell NPs. On the contrary, the small amount of DNA in the Au-(DNA-Ag)-Au trimers can only generate weak CD intensity though the Au-(DNA-Ag)-Au trimers has higher electric field. The HRTEM image of the Au-(DNA-Ag)-Au trimers (Figure 4B) showed that the Ag NPs grown between the gap of DNA had a polycrystalline structure dominated by the (111) facets (0.23 nm of lattice spacing), which was consistent with the results of optically active Au/(DNA-Ag) core–shell NPs.

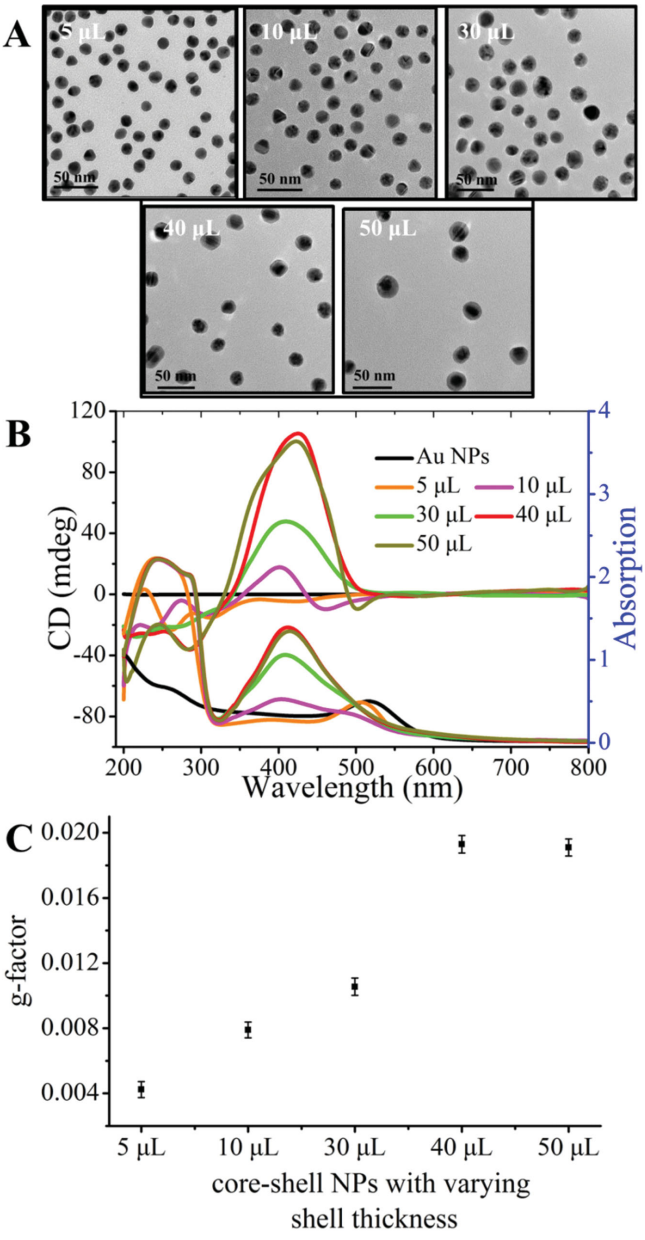

Figure 2. Growth of Au/(DNA-Ag) core–shell NPs with varying shell thickness by adding into various volume of $AgNO_3$ solution. A) Representative TEM images of Au/(DNA-Ag) core–shell NPs with $AgNO_3$ (0.75×10^{-3} M) solution of 5, 10, 30, 40, 50 μL, respectively. B) CD and UV–vis absorption spectra of Au/(DNA-Ag) core–shell NPs. C) *g*-factors of Au/(DNA-Ag) core–shell NPs with varying shell thickness.

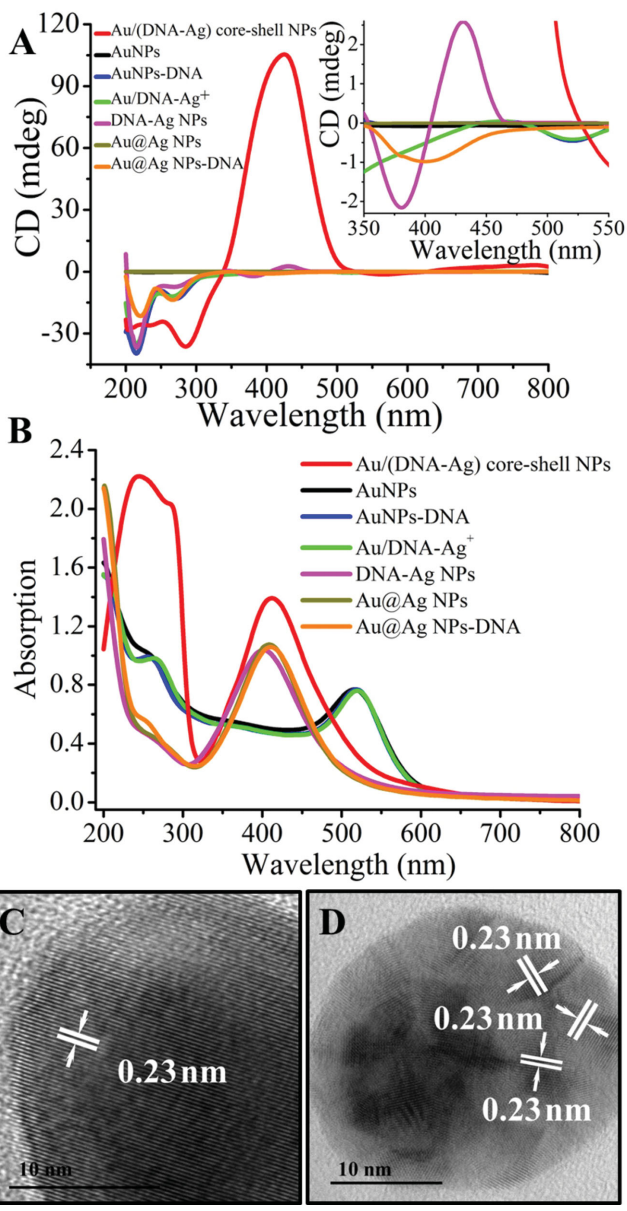

Figure 3. Chiroptical and geometric properties of Au/(DNA-Ag) core–shell NPs and their controls. A, B) CD A) and UV–vis absorption B) spectra of as-made Au NPs (Au NPs), Au NPs conjugated with DNA (Au NPs-DNA), Au NPs-DNA bound with Ag^+ (Au/DNA-Ag^+), Au/(DNA-Ag) core–shell NPs, Ag NPs grown on DNA template (DNA-Ag NPs), Ag shell deposited on the Au core without DNA (Au@Ag NPs), and Au@Ag NPs functionalized with DNA (Au@Ag NPs-DNA), respectively. Inset was the zoomed-in CD spectra of A). C,D) Representative HRTEM images of achiral Au@Ag NPs C), and optically active Au/(DNA-Ag) core–shell NPs D).

From the result of all the tested cases, therefore, the plasmonic optical activity of Au/(DNA-Ag) core–shell NPs is likely to be attributed to two aspects: (1) The plasmonic CD was induced by DNA-plasmon interaction,[2a,18c,19] including the DNA molecule orientation[2a,19b] and the embedding of the DNA, which is the dominant factor; and (2) the electromagnetic coupling and plasmonic oscillation between the core and shell, confirmed by electromagnetic simulation (Figure S9, Supporting Information), further amplified the plasmonic CD, and it was consistent with previous reports.[4d,9]

3. Conclusion

In summary, Au core-DNA-Ag shell NPs with distinctive chiroplasmonic performances have been successfully prepared for the first time. These novel NPs exhibited very intense CD activities in the visible range, with the highest *g*-factor value reported so far for the individual NPs with chiroplasmonic activity. Besides, the CD response of the individual Au core-DNA-Ag

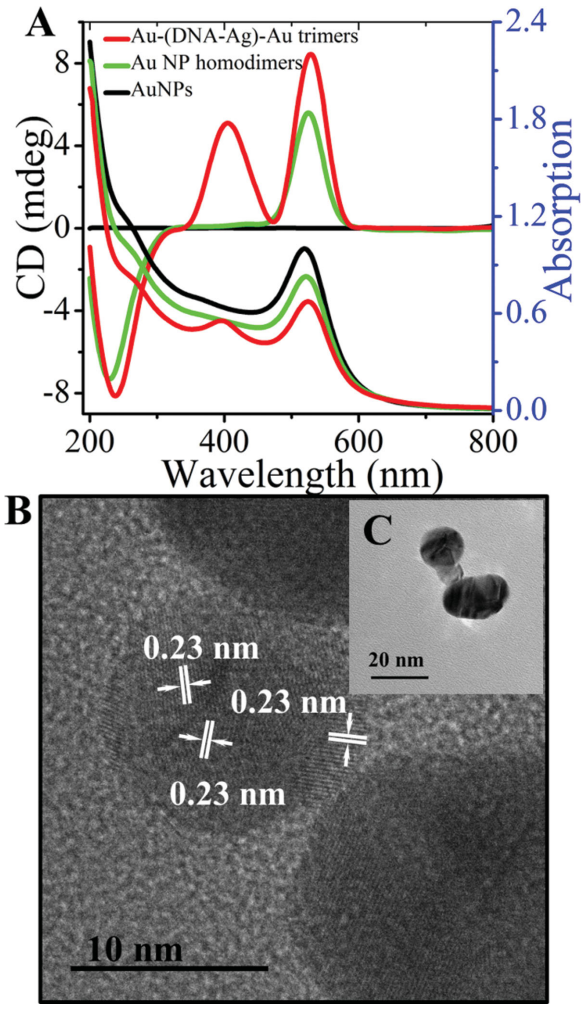

Figure 4. Chiroptical and geometric properties of Au-(DNA-Ag)-Au trimers and their controls. A) CD and UV–vis absorption spectra of Au-(DNA-Ag)-Au trimers, and their controls. B,C) Representative HRTEM B) and TEM C) image of Au-(DNA-Ag)-Au trimers.

shell NPs can be controllably manipulated by altering the Ag shell thickness. And their plasmonic chirogenesis was also illustrated, which was from the induction of DNA-plasmon interaction, and further amplification by the electromagnetic coupling of the core–shell structure. These unique optically active NPs may open up avenues for biosensing, chiral catalysis, the fabrication of "chirophotonic devices," and other potential applications. It is also expected that this synthesis approach can be extended to other kinds of chiral plasmonic NPs, nonplasmonic NPs, and composite NPs.

4. Experimental Section

Materials: Tetrachloroauric acid, trisodium citrate, silver nitrate, sodium borohydride, poly(vinylpyrrolidone) (PVP), ascorbic acid, and 4-nitrophenol were purchased from Sigma-Aldrich (St. Louis, MO, USA). All chemicals were used as received. Deionized (DI) water from a Milli-Q device (18.2 MΩ, Millipore, Molsheim, France) was used throughout this work. All glassware was cleaned with freshly prepared aqua regia and rinsed thoroughly with DI H2O prior to use. Thiolated DNA oligonucleotides purified by poly-acrylamide gel electrophoresis (PAGE) were purchased from Shanghai Sangon Biological Engineering Technology & Services Co. Ltd. (Shanghai, P.R. China) and suspended in DI water to a final concentration of 100×10^{-6} M. The DNA sequences are shown in Table S1, Supporting Information.

Synthesis of Au NPs: Two different sizes of Au NPs (20 ± 2.3 nm, 15 ± 0.8 nm) were used in this study, which were prepared through the reduction of $HAuCl_4$ by trisodium citrate, according to previous research.[14,20] In brief, trisodium citrate solution (2.0 or 2.2 mL, 1% by weight, freshly prepared) was quickly added to a boiling solution of $HAuCl_4$ (100 mL, 0.25×10^{-3} M) under vigorous stirring and refluxed for 20 min until the color of the solution changed from blue to stable wine red. The reaction solution was subsequently cooled to room temperature before being stored at 4 °C.

Synthesis of Au/(DNA-Ag) Core–Shell NPs: To prepare Au/(DNA-Ag) core–shell NPs, as-prepared Au NPs (15 ± 0.8 nm) were added to ssDNA (DNA 1 in Table S1, Supporting Information, 2×10^{-6} M).[5d,6a,b,21] After incubation for 12 h at room temperature,[18c] the Au NPs-DNA conjugates were centrifuged to remove the redundant DNA, and resuspended in the original volume of 100×10^{-3} M phosphate buffer. Silver nitrate ($AgNO_3$, 0.75×10^{-3} M) was added to the Au NPs-DNA conjugation solution and incubated for 12 h in the dark, at a corresponding volume (5, 10, 30, 40, or 50 μL), followed by additional centrifugation to remove excess ions. The precipitated pellet was redispersed into a solution containing 0.5% of PVP (as a stabilizer), and reduced by 20 μL 0.5 M of ascorbic acid to form core–shell NPs with varying silver thickness.[12b] The reaction solution was shaken for 3 h at room temperature and then centrifuged. The precipitate was washed three times and resuspended in 100 μL Millipore-Q water.

Synthesis of Au@Ag NPs: The Au@Ag NPs were synthesized according to the procedures of Au/(DNA-Ag) core–shell NPs described above, but without ssDNA and centrifugation which was performed to remove excess ions before reduction. The volume of added $AgNO_3$ solution for both was 40 μL.

Synthesis of DNA-Ag NPs: Silver nitrate (0.75×10^{-3}M, 40 μL) was added to the cytosine rich-ssDNA[5c,6e] (DNA 1 in Table S1, Supporting Information, 2×10^{-6} M) solution with 0.5% of PVP stabilizer. After incubation for 12 h at room temperature, reduction was carried by the addition of 20 μL of 0.5 M ascorbic acid and shaking for 3 h. The reaction solution was then centrifuged, leaving the precipitated pellet (DNA-Ag NPs) resuspended in Millipore-Q water for use.

Assembly of Au NP Homodimers and Au-(DNA-Ag)-Au Trimers: To prepare the Au NP homodimers, the as-made Au NPs (20 ± 2.3 nm) were first functionalized with complementary DNA sequences (DNA 21 and DNA 22 in Table S1, Supporting Information) in a molar ratio of 1:1, respectively. Then we mixed these two conjugated Au NP-DNA solutions with 50×10^{-3}M NaCl which were incubated for 12 h at room temperature. After centrifugation and resuspension, we obtained Au NP homodimers. For Au-(DNA-Ag)-Au trimers, an additional process of Ag NPs growth between the gap of Au NP homodimers was employed.[6b,21] Briefly, silver nitrate (0.75×10^{-3}M, 40 μL) was added to the pre-assembled Au NP homodimers solution. After incubation for 12 h in the dark at room temperature and removing excess ions, they were reduced by 20 μL of 0.5 M ascorbic acid with 0.5% of PVP stabilizer to form the Au-(DNA-Ag)-Au trimers.

Electromagnetic Simulations: Computer simulations of electromagnetic field were performed using CST Microwave Studio. The propagation of excitation beam was defined in the *z*-axis direction, in which the electric field of the light beam was set in the *y*-axis direction with initial values of 1 V m^{-1}. The simulated electric field reached values of 52.1 and 8.87 V m^{-1} for Au-(DNA-Ag)-Au trimers and Au@Ag NPs, respectively (Figure S9, Supporting Information).

Characterization: Images were obtained using a transmission electron microscope (JEOL JEM-2100) operating at an acceleration voltage of 200 kV. The size distributions were measured using a Zetasizer Nano ZS system (Malvern) with a 633 nm laser. All UV–vis results were acquired on a UNICO 2100 PC UV–vis spectrophotometer and processed using Origin Lab software. Chiral spectra were obtained by

MOS-450/AF-Circular dichroism. Energy dispersive X-ray spectroscopy (EDX) spectra were carried out using a Tecnai G2 F20 S-Twin electron microscope, equipped with an electron beam monochromator and energy dispersive X-ray spectroscopy.

Calculation of the Anisotropy Factor (g-Factor): The anisotropy factor was calculated as, $g = \Delta A/A = \theta\,[\text{mdeg}]/(32980 \times A)$, θ[mdeg] and A were the chiral intensity of samples and the corresponding absorption.[1a]

Supporting Information

Supporting Information is available from the Wiley Online Library or from the author.

Acknowledgements

X.W. and L.X. contributed equally to this paper. This work is financially supported by NSFC (Grant Nos. 21101079, 21371081, and 21301073).

Received: September 11, 2014
Revised: November 28, 2014
Published online: December 18, 2014

[1] a) I. Dolamic, S. Knoppe, A. Dass, T. Bürgi, *Nat. Commun.* **2012**, *3*, 798; b) C. Zeng, T. Li, A. Das, N. L. Rosi, R. Jin, *J. Am. Chem. Soc.* **2013**, *135*, 10011; c) A. Sánchez-Castillo, C. Noguez, I. L. Garzón, *J. Am. Chem. Soc.* **2010**, *132*, 1504; d) P. Graf, A. Mantion, A. Haase, A. F. Thünemann, A. Mašić, W. Meier, A. Luch, A. Taubert, *ACS Nano* **2011**, *5*, 820; e) Y. Cui, Y. Wang, R. Liu, Z. Sun, Y. Wei, Y. Zhao, X. Gao, *ACS Nano* **2011**, *5*, 8684; f) I. Lieberman, G. Shemer, T. Fried, E. M. Kosower, G. Markovich, *Angew. Chem. Int. Ed.* **2008**, *47*, 4855; g) Y. Pei, S. Lin, J. Su, C. Liu, *J. Am. Chem. Soc.* **2013**, *135*, 19060; h) M. Zhu, H. Qian, X. Meng, S. Jin, Z. Wu, R. Jin, *Nano Lett.* **2011**, *11*, 3963.

[2] a) F. Lu, Y. Tian, M. Liu, D. Su, H. Zhang, A. O. Govorov, O. Gang, *Nano Lett.* **2013**, *13*, 3145; b) J. M. Slocik, A. O. Govorov, R. R. Naik, *Nano Lett.* **2011**, *11*, 701.

[3] a) Y. Wang, J. Xu, Y. Wang, H. Chen, *Chem. Soc. Rev.* **2013**, *42*, 2930; b) C. Wolf, K. W. Bentley, *Chem. Soc. Rev.* **2013**, *42*, 5408; c) E. Plum, J. Zhou, J. Dong, V. A. Fedotov, T. Koschny, C. M. Soukoulis, N. I. Zheludev, *Phys. Rev. B* **2009**, *79*, 035407.

[4] a) A. J. Mastroianni, S. A. Claridge, A. P. Alivisatos, *J. Am. Chem. Soc.* **2009**, *131*, 8455; b) Z. Li, Z. Zhu, W. Liu, Y. Zhou, B. Han, Y. Gao, Z. Tang, *J. Am. Chem. Soc.* **2012**, *134*, 3322; c) J. Shen, L. Xu, C. Wang, H. Pei, R. Tai, S. Song, Q. Huang, C. Fan, G. Chen, *Angew. Chem. Int. Ed.* **2014**, *53*, 8338; d) A. Kuzyk, R. Schreiber, Z. Fan, G. Pardatscher, E.-M. Roller, A. Högele, F. C. Simmel, A. O. Govorov, T. Liedl, *Nature* **2012**, *483*, 311; e) X. Shen, A. Asenjo-Garcia, Q. Liu, Q. Jiang, F. J. García de Abajo, N. Liu, B. Ding, *Nano Lett.* **2013**, *13*, 2128.

[5] a) C. F. Monson, A. T. Woolley, *Nano Lett.* **2003**, *3*, 359; b) J. Timper, K. Gutsmiedl, C. Wirges, J. Broda, M. Noyong, J. Mayer, T. Carell, U. Simon, *Angew. Chem. Int. Ed.* **2012**, *51*, 7586; c) T. Vosch, Y. Antoku, J.-C. Hsiang, C. I. Richards, J. I. Gonzalez, R. M. Dickson, *Proc. Natl. Acad. Sci. U.S.A.* **2007**, *104*, 12616; d) J. T. Petty, B. Giri, I. C. Miller, D. A. Nicholson, O. O. Sergev, T. M. Banks, S. P. Story, *Anal. Chem.* **2013**, *85*, 2183; e) P. Shah, A. Rørvig-Lund, S. B. Chaabane, P. W. Thulstrup, H. G. Kjaergaard, E. Fron, J. Hofkens, S. W. Yang, T. Vosch, *ACS Nano* **2012**, *6*, 8803.

[6] a) P. R. O'Neill, K. Young, D. Schiffels, D. K. Fygenson, *Nano Lett.* **2012**, *12*, 5464; b) S. Shukla, M. Sastry, *Nanoscale* **2009**, *1*, 122; c) E. G. Gwinn, P. O'Neill, A. J. Guerrero, D. Bouwmeester, D. K. Fygenson, *Adv. Mater.* **2008**, *20*, 279; d) J. T. Petty, O. O. Sergev, D. A. Nicholson, P. M. Goodwin, B. Giri, D. R. McMullan, *Anal. Chem.* **2013**, *85*, 9868; e) G. Shemer, O. Krichevski, G. Markovich, T. Molotsky, I. Lubitz, A. B. Kotlyar, *J. Am. Chem. Soc.* **2006**, *128*, 11006.

[7] J. Wu, Y. Fu, Z. He, Y. Han, L. Zheng, J. Zhang, W. Li, *J. Phys. Chem. B* **2012**, *116*, 1655.

[8] T. Molotsky, T. Tamarin, A. B. Moshe, G. Markovich, A. B. Kotlyar, *J. Phys. Chem. C* **2010**, *114*, 15951.

[9] Y. Zhao, L. Xu, W. Ma, L. Wang, H. Kuang, C. Xu, N. A. Kotov, *Nano Lett.* **2014**, *14*, 3908.

[10] a) H. D. Hill, J. E. Millstone, M. J. Banholzer, C. A. Mirkin, *ACS Nano* **2009**, *3*, 418; b) I. C. Pekcevik, L. C. H. Poon, M. C. P. Wang, B. D. Gates, *Anal. Chem.* **2013**, *85*, 9960.

[11] Y. Fu, J. Zhang, X. Chen, T. Huang, X. Duan, W. Li, J. Wang, *J. Phys. Chem. C* **2011**, *115*, 10370.

[12] a) D.-K. Lim, K.-S. Jeon, H. M. Kim, J.-M. Nam, Y. D. Suh, *Nat. Mater.* **2010**, *9*, 60; b) J.-H. Lee, J.-M. Nam, K.-S. Jeon, D.-K. Lim, H. Kim, S. Kwon, H. Lee, Y. D. Suh, *ACS Nano* **2012**, *6*, 9574; c) O. Pena-Rodriguez, U. Pal, *Nanoscale* **2011**, *3*, 3609.

[13] a) U. Tohgha, K. K. Deol, A. G. Porter, S. G. Bartko, J. K. Choi, B. M. Leonard, K. Varga, J. Kubelka, G. Muller, M. Balaz, *ACS Nano* **2013**, *7*, 11094; b) J. George, K. G. Thomas, *J. Am. Chem. Soc.* **2010**, *132*, 2502; c) B. M. Maoz, R. van der Weegen, Z. Fan, A. O. Govorov, G. Ellestad, N. Berova, E. W. Meijer, G. Markovich, *J. Am. Chem. Soc.* **2012**, *134*, 17807; d) R. Kobayashi, Y. Nonoguchi, A. Sasaki, H. Yao, *J. Phys. Chem. C* **2014**, *118*, 15506; e) C. Gautier, T. Bürgi, *J. Am. Chem. Soc.* **2006**, *128*, 11079.

[14] X. Wu, L. Xu, L. Liu, W. Ma, H. Yin, H. Kuang, L. Wang, C. Xu, N. A. Kotov, *J. Am. Chem. Soc.* **2013**, *135*, 18629.

[15] a) A. Ben-Moshe, B. M. Maoz, A. O. Govorov, G. Markovich, *Chem. Soc. Rev.* **2013**, *42*, 7028; b) Z. Xu, L. Xu, L. M. Liz-Marzán, W. Ma, N. A. Kotov, L. Wang, H. Kuang, C. Xu, *Adv. Opt. Mater.* **2013**, *1*, 626.

[16] a) S. Gómez-Graña, B. Goris, T. Altantzis, C. Fernández-López, E. Carbó-Argibay, A. Guerrero-Martínez, N. Almora-Barrios, N. López, I. Pastoriza-Santos, J. Pérez-Juste, S. Bals, G. Van Tendeloo, L. M. Liz-Marzán, *J. Phys. Chem. Lett.* **2013**, *4*, 2209; b) Y. Ma, W. Li, E. C. Cho, Z. Li, T. Yu, J. Zeng, Z. Xie, Y. Xia, *ACS Nano* **2010**, *4*, 6725.

[17] C. Li, L. Sun, Y. Sun, T. Teranishi, *Chem. Mater.* **2013**, *25*, 2580.

[18] a) W. Ma, H. Kuang, L. Xu, L. Ding, C. Xu, L. Wang, N. A. Kotov, *Nat. Commun.* **2013**, *4*, 2689; b) W. Ma, H. Kuang, L. Wang, L. Xu, W.-S. Chang, H. Zhang, M. Sun, Y. Zhu, Y. Zhao, L. Liu, C. Xu, S. Link, N. A. Kotov, *Sci. Rep.* **2013**, *3*, 1934; c) W. Yan, W. Ma, H. Kuang, L. Liu, L. Wang, L. Xu, C. Xu, *J. Phys. Chem. C* **2013**, *117*, 17757; d) Y. Zhao, L. Xu, W. Ma, L. Wang, H. Kuang, C. Xu, N. A. Kotov, *Nano Lett.* **2014**, *14*, 3908.

[19] a) C. Hao, L. Xu, W. Ma, L. Wang, H. Kuang, C. Xu, *Small* **2014**, *10*, 1805; b) H. Zhang, A. O. Govorov, *Phys. Rev. B* **2013**, *87*, 075410; c) A. O. Govorov, Z. Fan, P. Hernandez, J. M. Slocik, R. R. Naik, *Nano Lett.* **2010**, *10*, 1374; d) L. Xu, C. Hao, H. Yin, L. Liu, W. Ma, L. Wang, H. Kuang, C. Xu, *J. Phys. Chem. Lett.* **2013**, *4*, 2379.

[20] W. Yan, L. Xu, C. Xu, W. Ma, H. Kuang, L. Wang, N. A. Kotov, *J. Am. Chem. Soc.* **2012**, *134*, 15114.

[21] Z. Huang, F. Pu, D. Hu, C. Wang, J. Ren, X. Qu, *Chem. Eur. J.* **2011**, *17*, 3774.